Article

Role of Vanadium Addition on Hot Deformation Behavior of Aluminum Alloy 5083

Lijuan Wang [1,2], Xiangjie Wang [1,*], Xiao Zhu [3], Xin Xu [3], Jianzhong Cui [1], Bin Liao [4], Xiaodong Wang [5] and Xiaodong Wu [4,*]

[1] Key Laboratory of Electromagnetic Processing of Materials, Ministry of Education, Northeastern University, Shenyang 110819, China

[2] Application Technology Department, Chinalco Materials Application Research Institute Co. Ltd., Beijing 100083, China

[3] Research and Development Department, Zhongwang Group Co. Ltd., Liaoyang 111003, China

[4] International Joint Laboratory for Light Alloys (Ministry of Education), College of Materials Science and Engineering, Chongqing University, Chongqing 400044, China

[5] National Joint Engineering Research Center for Abrasion Control and Molding of Metal Materials, Henan University of Science and Technology, Luoyang 471003, China

[*] Correspondence: wangxj@epm.neu.edu.cn (X.W.); xiaodongwu@cqu.edu.cn (X.W.);
Tel.: +86-18640394973 (X.W.); +86-23-6512-7306 (X.W.) Fax:+86-23-6512-7306 (X.W.); +86-24-8368-1758 (X.W.)

check for updates

Abstract: The effect of V addition on the hot deformation behavior of AA5083 was investigated. Single axial compression tests were conducted on the cast and homogenized samples with strain rates ranging from 0.01 to 10 s^{-1} and deformation temperatures ranging from 300 to 450 °C. The results showed that the contents of V (0–0.10, in wt.%) do not change the grain size of alloy 5083 significantly in the as cast and homogenized conditions, but the formation of fine Al$_3$V particles in the alloy with an addition of 0.05 wt.% V can increase the flow stress, and its activation energy is 10.0% higher than that of V-free alloy 5083. The processing maps show that the appropriate process domain for alloy 5083 with 0.05 wt.% V changes at different true strains. The mechanism for deformation softening is discussed as well.

1. Introduction

Aluminum alloy 5083 has been widely used for manufacturing dies, aircraft body panels, ship panels and automotive panels due to its high strength and formability [1]. Generally, aluminum alloy 5083 is processed by rolling, extrusion or forging. Hot deformation has been an effective way to change the phase transformation kinetics [2], and if it is done at high pressure, the stability of phases will be influenced as well [3]. The thermal simulation technique can test materials under dynamic thermal-mechanical loading, replicate real manufacturing process in the laboratory, and has been widely utilized to study the hot-formability and microstructure of aluminum alloys [4,5]. It is documented that the hot deformation behavior of aluminum alloys is affected by alloying elements [6–8], as the addition of solute elements may increase the dislocation density and hinder the dislocation motion. Thus, the mobility of grain boundaries is reduced [9,10]. The contribution from the work hardening and dynamic softening operates during the hot deformation process [11–15].

It has been reported that the addition of V has a significant effect on the microstructure and properties of aluminum alloys [16–21]. For example, Esquivel and Gupta [19] found that the hardness of Al-*x*V alloys increased with a higher V content, which was caused by the solid solution strengthening

effect resulted from the high solid solubility of V and grain refinement. Shi et al. [20] investigated the hot deformation behavior of aluminum alloy 7150 with different V contents and found that the flow stress increased significantly with V additions. The activation energy increased from 229 kJ/mol for the base alloy to 270 kJ/mol for the one containing 0.05 wt.% V, due to the delay of dynamic recrystallization in the latter. Chen et al. [21] studied the effect of Zr and V contents on the hot deformation of alloy 7150 and found that adding 0.05 wt.% V could significantly enhance the activation energy of this alloy deformed at 300–350 °C. However, the effect of V on the activation energy of alloy 5083 has not been investigated. The hot deformation mechanism of this series of alloys is unclear as well.

Therefore, in this study, the effect of V content on the hot deformation behavior of aluminum alloy 5083 was systematically investigated. Single axial compression tests were employed and the activation energy was calculated as a function of V content. The formation of V-containing particles was discussed as well.

2. Materials and Methods

2.1. Materials

Aluminum alloys 5083 with four different V contents (0–0.10 wt.%, Table 1) were prepared by vacuum electromagnetic casting to approximate dimensions $50 \times 100 \times 200$ mm^3, and the composition was measured by using an optical emission spectrometer. All these ingots were homogenized at 400 °C for 4 h, followed by 500 °C for 24 h, and then cut along the casting direction into rods with a diameter of 8 mm and length of 15 mm for compression tests.

Table 1. Chemical composition of experimental alloys (in wt.%).

Alloy	Si	Fe	Cu	Mn	Mg	Ni	Ti	Zr	V	Al
A	0.04	0.05	0.01	0.7	4.65	0.15	0.01	0.12	0	Bal.
B	0.04	0.05	0.01	0..7	4.65	0.15	0.01	0.12	0.03	Bal.
C	0.04	0.05	0.01	0.7	4.65	0.15	0.01	0.12	0.05	Bal.
D	0.04	0.05	0.01	0..7	4.65	0.15	0.01	0.12	0.10	Bal.

2.2. Methods

Single axial compression tests (Figure 1) were carried out by using a thermo-simulation testing machine MMS-100 (Key Laboratory of rolling and automation, Shenyang, China) at strain rates of 0.01, 0.1, 1 and 10 s^{-1} and deformation temperatures of 300, 350, 400 and 450 °C, respectively. The samples were heated to the required temperature at a rate of 10 °C/s and soaked for 1 min to make sure the temperature of the samples was evenly distributed. When the true strain of the samples reached 0.7, the sample was air-cooled immediately at a cooling rate of about 20 °C/s. Lubrication between the anvil and sample was used to minimize friction at the sample/die interface during deformation. The Vickers hardness was measured with a 1 kg load, and generally 7–10 indents were taken for the calculation of average values and experimental errors.

The microstructure of as-cast, homogenized and deformed samples was observed by using light optical microscopy (LM, AxioImager M2M, Carl Zeiss AG, Oberkochen, Germany) and transmission electron microscopy (TEM, Philips CM-12, Royal Dutch Philips Electronics Ltd. Amsterdam, Holland). LM samples were first ground on the emery paper and then electropolished in a solution of 20 vol.% HClO$_4$ and 80 vol.% C$_2$H$_5$OH at 18 V for 40–50 s. TEM samples were machined as Φ 3 mm plates, ground to the thickness of 80–90 μm, and electropolished using the electrolyte of 30 vol.% HNO$_3$ and 70 vol.% CH$_3$OH at −30 °C. The TEM electropolishing was carried out at a voltage of 15 V for 60 s. Processing maps were generated to determine the appropriate domains for hot working.
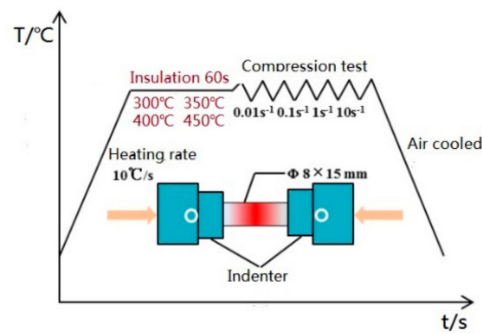
Figure 1. Schematic diagram of compression tests.

3. Results and Discussion

3.1. Microstructure of the 5083 + V Alloy before Hot Compression

The as-cast microstructure of the studied alloys was examined by using light optical microscopy, and no significant difference in grain sizes was observed for alloys containing different contents of V. After homogenization, the hardness of all alloys reached the level of 88 ± 2 HV1. Most of the grain sizes were less than 400 μm (Figure 2), and the alloy with a higher V addition seemed to have relatively smaller and uniform grains, especially the one with 0.05 wt.% V (Figure 2c).
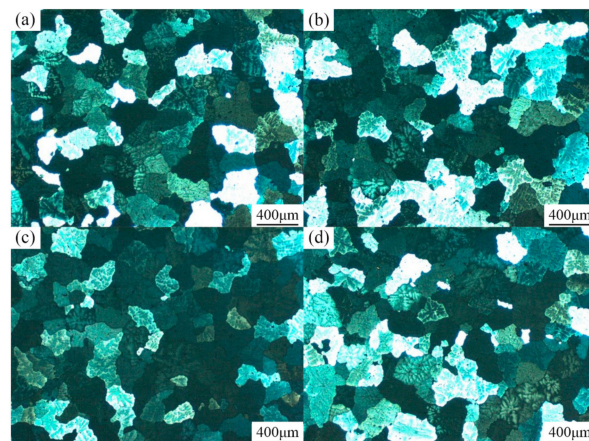
Figure 2. Light optical micrographs of homogenized samples: (**a**) 5083, (**b**) 5083 + 0.03 wt.% V, (**c**) 5083 + 0.05 wt.% V and (**d**) 5083 + 0.10 wt.% V.

In order to understand the influence of V addition on the homogenized alloys, the microstructure was further examined at a magnified scale under TEM (Figure 3). It shows that for the alloy with 0–0.03 wt.% V, no V-containing particles can be detected. When the V addition reaches 0.05 wt.%, V-containing particles with a diameter of 10–50 nm emerge. The selected area diffraction (SAD) pattern indicates that these particles are Al_3V phases with a simple cubic structure, as shown from spot A in Figure 3c. They are coherent or semi-coherent with the matrix.

Furthermore, some lath-like phases can also be observed, shown as spot B in Figure 3d. According to EDX analysis, these phases contain Mn and Fe, and match the SAD of $(Mn, Fe)Al_6$ phase, which is of base-centered orthorhombic structure in the space group of Ccmm (63) with lattice constants of a = 0.7498 nm, b = 0.6495 nm and c = 0.8837 nm.
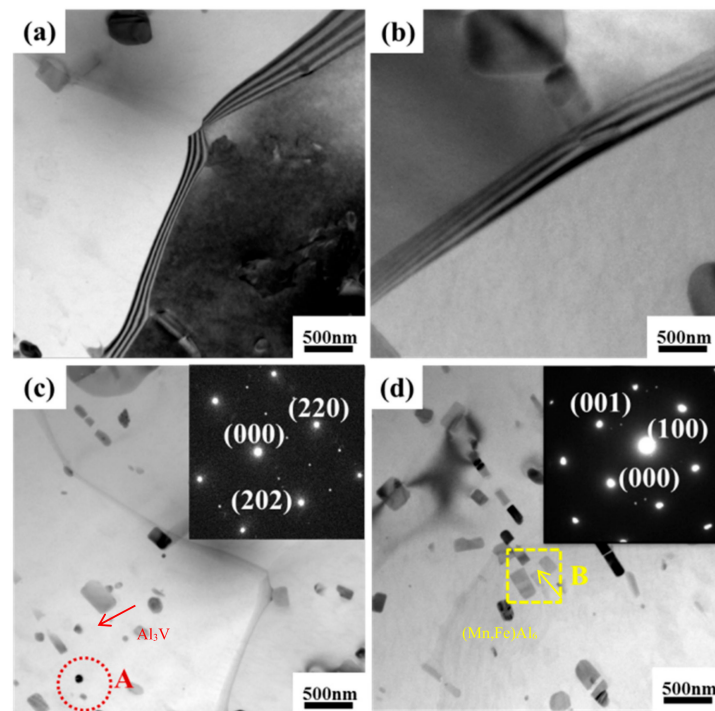
Figure 3. TEM bright field images of the homogenized aluminum alloys: (**a**) 5083, (**b**) 5083 + 0.03 wt.% V, (**c**) 5083 + 0.05 wt.% V and (**d**) 5083 + 0.10 wt.% V.

3.2. Stress-Strain Curves and Microstructure of Hot Compressed Alloy

True stress-true strain curves obtained during hot compression for different V-containing 5083 alloys at various temperatures and strain rates are shown in Figure 4. When the compression tests are performed at 400 °C with a strain rate of 0.01 s^{-1}, the addition of V to alloy 5083 seems to increase the flow stress, especially for alloy C (5083 + 0.05 wt.% V), the peak stress reaches a maximum value. The peak stress hardly increases in alloy D with the V content as high as 0.10 wt.% (Figure 4a). It can be deduced that adding V (≤0.05 wt.%) to alloy 5083 may result in a higher work hardening rate than deformation softening, which leads to the gradual increase of peak stresses with V content. When the V reaches 0.10 wt.%, the work hardening resulting from dislocation multiplication is not as much as that in alloy C, so the peak stress of alloy D is relatively lower.

For a given alloy, e.g., alloy C, the flow behavior is influenced by strain rates and deformation temperatures (Figure 4b–e). It can be seen that the level of the flow stress consistently decreases with increasing deformation temperature. For each curve, the flow stress generally increases rapidly with increasing strain at the beginning of hot compression, reaches the peak stress and then decreases slightly to a near constant value, which is most remarkable at lower strain rates. Such a phenomenon indicates that at the early stage of plastic deformation, the work hardening caused by dislocation multiplication is predominant over the dynamic softening resulting from dynamic recovery and recrystallization. After the peak, the stress may decrease due to a predominant dynamic softening effect and later the value may be constant due to a good balance between work hardening and dynamic softening. The flow stress tends to increase at a higher strain rate or lower deformation temperature. When the deformation happens at a low strain rate, there is sufficient time for dynamic recovery and recrystallization, which leads to the softening of alloys.
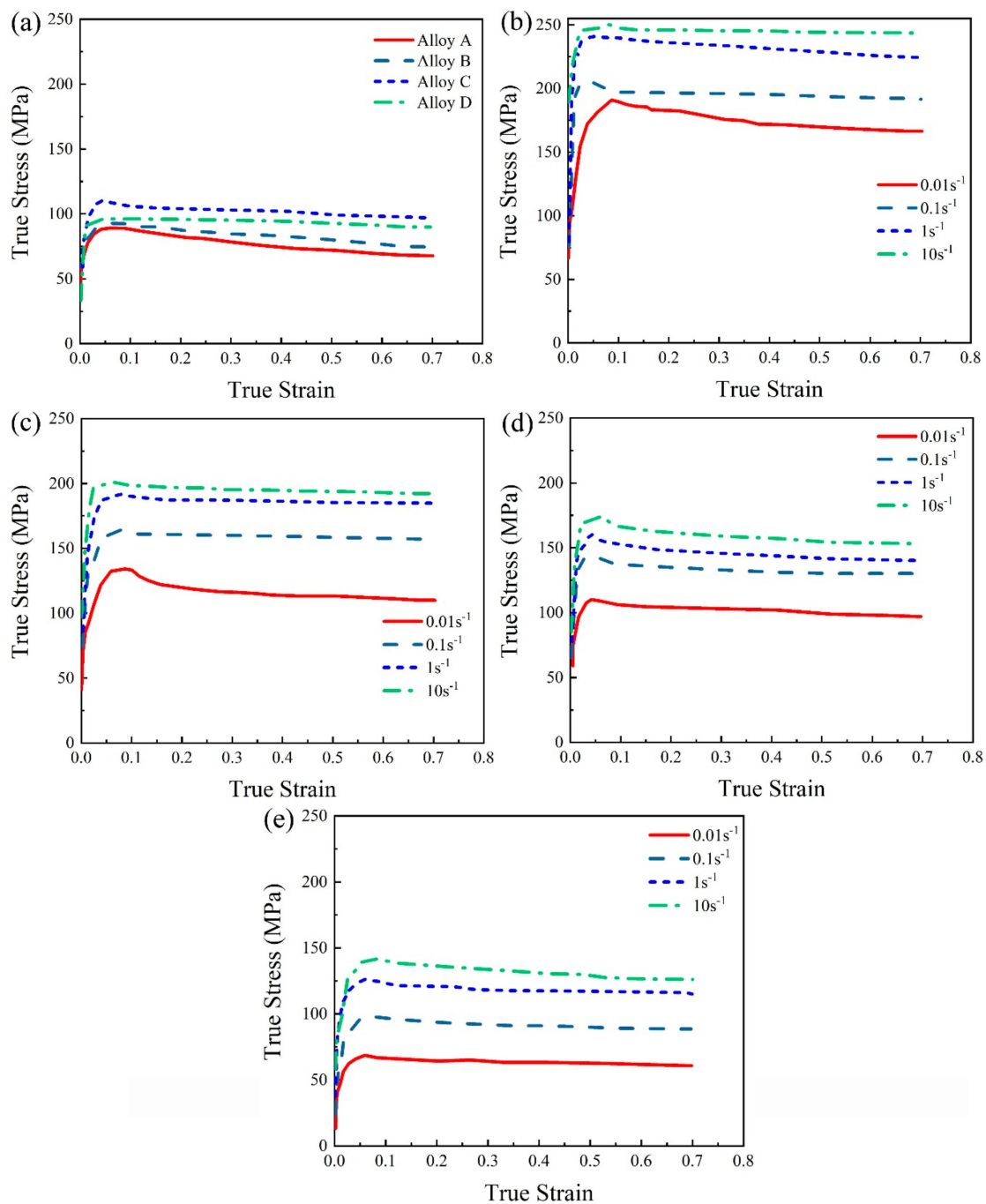
Figure 4. True stress–true strain curves of alloys during hot deformation after homogenization (**a**) alloy 5083 with various V contents compressed at 400 °C and 0.01 s^{-1}, (**b**–**e**) alloy C compressed at different temperatures and strain rates (**b**) 300 °C, (**c**) 350 °C, (**d**) 400 °C and (**e**) 450 °C.

As seen in Figure 4a, alloy 5083 with V additions shows higher flow stress and peak stress, which is relate to the delay of the dynamic softening by the presence of Al$_3$V particles. Figure 5 shows the TEM bright field images of the alloys deformed at 400 °C and a strain rate of 0.1 s^{-1}. The second phase particles can hardly be observed in alloy 5083 without V (Figure 5a) and alloy 5083 with 0.03 wt.% V (Figure 5b). For alloy 5083 with 0.1 wt.% V (Figure 5c), it seems that the Al$_3$V particles presented in the homogenized condition (Figure 3c) can inhibit the dynamic recrystallization process during hot deformation and increase the flow stress accordingly (Figure 5c). It can be expected that the moving dislocations may bend at the edge of Al$_3$V phases, which results in a strong pinning effect on the

dislocation gliding. Moreover, the low angle grain boundaries can be fixed by the dispersed phases, which will decrease the rotational capacity of the sub-grains and therefore suppress the dynamic recovery in the alloy. When the V content in alloy 5083 increases to 0.10 wt.%, the coarse dispersoids may emerge and inhomogeneously distribute (marked by red arrow, Figure 5d), which normally makes no effective contribution to the work hardening of aluminum alloys [22], thus the flow stress is not increased further.
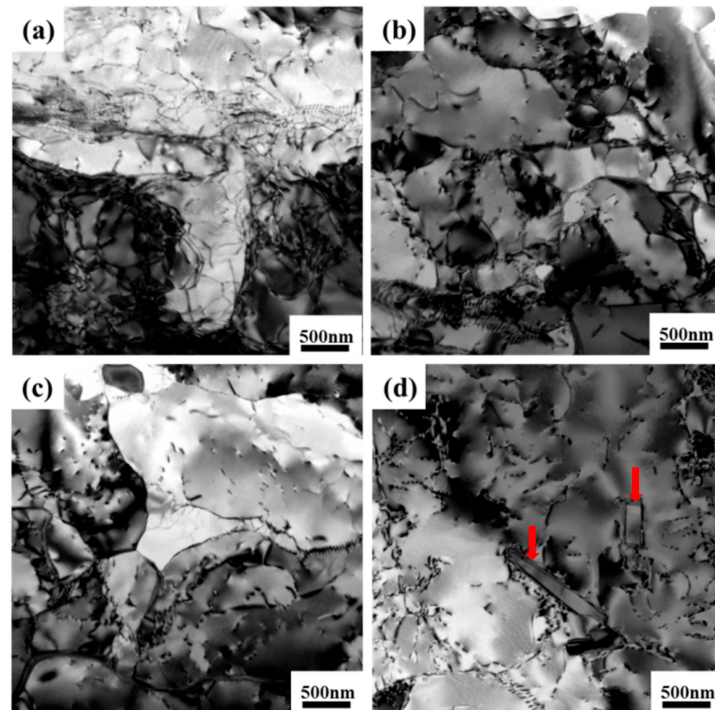
Figure 5. TEM bright field images of aluminum alloys after hot compression: (**a**) 5083, (**b**) 5083 + 0.03 wt.% V, (**c**) 5083 + 0.05 wt.% V and (**d**) 5083 + 0.10 wt.% V.

TEM images of aluminum alloy 5083 containing 0.05 wt.% V are shown in Figure 6 with a strain rate of 0.01 s^{-1} at a deformation temperature of 300–450 °C. It is observed that severe deformation causes dislocation pile-up in a high density, leading to the destruction of grain boundaries. The accumulation of dislocation promotes the formation of dislocation tangles, which were regularly arranged between cell boundaries.

As shown in Figure 6, small dispersed Al$_3$V particles tend to grow up with the increase of deformation temperature. Some dislocations presented in the cellular of sub-structure grains are hard to move due to the pinning effect of the fine precipitated phases (Figure 6b). A typical dynamic recovery process occurs when the deformation temperature rises to 400 °C, as indicated from the true stress–true strain curves in Figure 4d. The dislocations are redistributed and the sub-grain boundaries are formed. Afterwards, the dynamic recovery process is continued. The dislocation density decreases significantly with the increase of deformation temperature (Figure 6c), which is why the flow stress is decreased accordingly. Meanwhile, Al$_3$V particles can be observed clearly in the grains, which may hinder the movement of grain boundaries and inhibit the growth of the recrystallization nucleus (Figure 6d).
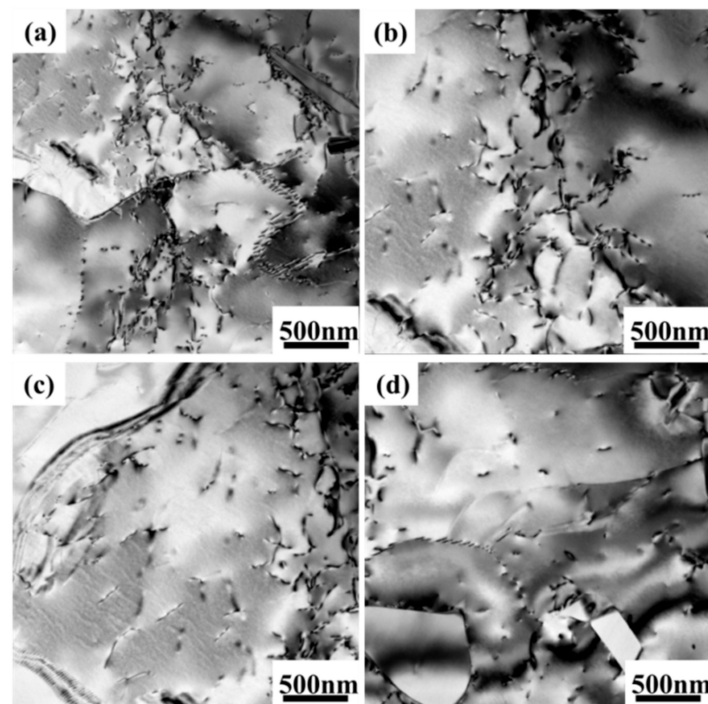
Figure 6. TEM images of aluminum alloy 5083 containing 0.05 wt.% V at different deformation temperatures: (**a**) 300 °C, (**b**) 350 °C, (**c**) 400 °C, and (**d**) 450 °C.

3.3. Constitutive Equation and Processing Map

In order to further understand the influence of V on the hot deformation behavior of alloy 5083, the activation energy for each process can be figured out.

It is well documented that the flow stress of hot deformation of metal materials mainly depends on strain ε, temperature T and strain rate E [23,24], which can be described by the relationship from the Arrhenius equation proposed by Sellars and Tegart [25]:

$$E = A[\sin h[\alpha\sigma]]^{n} \exp(-Q/RT) \tag{1}$$

where E is the strain rate, A is the structure factor (s^{-1}), α is the pressure level (MPa), n is the stress exponent, Q is the activation energy (J/mol), R is the universal constant and T is the deformation temperature (K).

According to the hyperbolic sine function form of the Arrhenius equation, Taylor's expansion can be adopted as follows:

$$\sin h(x) = \frac{e^{x} - e^{-x}}{2} = x + \frac{x^3}{3!} + \frac{x^5}{5!} + \cdots \tag{2}$$

where $x = \alpha\sigma$ when the material is at a low stress level ($x \leq 0.8$). When $\sin hx \rightarrow x$, Equation (1) can be expressed as:

$$E = A_1\sigma^{n_1} \exp(-Q/RT) \tag{3}$$

where $A_1 = A\alpha^{n1}$.

When the material is at a high stress level ($x \geq 1.2$), e^{-x} can be ignored and Equation (1) can be expressed as:

$$E = A_2 \exp(\beta\sigma) \exp(-Q/RT) \tag{4}$$

In the formula above, $A_2 = A/2^n$ and $\beta = \alpha n1$.

Within the entire range of stress levels, Equation (4) can be expressed as:

$$E = A[\sin h[\alpha\sigma]]^n \exp(-Q/RT)$$ (5)

At a given temperature, Equations (3)–(5) can be simplified as:
At low stress level:

$$lnE = lnA_1 + n_1 \ln\sigma - Q/RT$$ (6)

At high stress level:

$$lnE = lnA_2 + \beta\sigma - Q/RT$$ (7)

Within the entire stress level:

$$lnE = lnA - Q/RT + nln[\sin[\alpha\sigma]]$$ (8)

Activation energy is an important indicator to evaluate the resistance of material to deformation during the hot deformation process, and its value depends on the initial state and the composition of the alloy. In this paper, the activation energy Q of the material is derived from the experimental data of alloy C. When the alloy reaches the dynamic equilibrium stage between work hardening and dynamic recovery, the peak flow stress σ_p is usually expressed as σ. The pressure multiple α is defined as $\alpha = \beta/n_1$, where β is the average slope of the $\ln(E)-\sigma_p$ curve in different temperature ranges, and n_1 is the average slope of the $\ln(E)-\ln(\sigma_p)$ curve in different temperature ranges. The values of β and n_1 can be calculated from Figure 7 and the α value of alloy C is determined to be 0.00635.
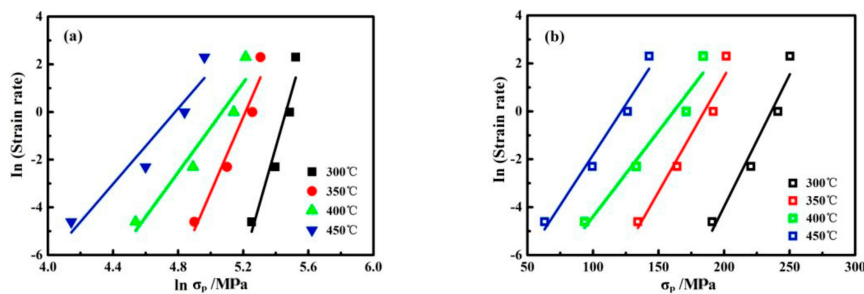
Figure 7. Relationship between (**a**) *ln E* and *lnσ_p* and (**b**) *ln E* and *σ_p*.

The following equation is obtained from the partial differentiation of Equation (8):

$$Q = R\left[\frac{\partial lnE}{\partial ln[\sinh[\alpha\sigma_p]]}\right]_T\left[\frac{\partial \ln[\sinh[\alpha\sigma_p]]}{\partial[1/T]}\right]_{\dot{\varepsilon}}$$ (9)

where n denotes as the average slope of the $\ln E$-$\ln(\sinh(\alpha\sigma_p))$ curve at different temperatures and S represents the average slope of the $ln(sinh(\alpha\sigma_p))-1/T$ curve at different strain rates.

Figure 8a shows the relationship between lnE and $ln(sinh(\alpha\sigma_p))$ derived from the measured peak stresses. The average value n of the slope is calculated at different deformation temperatures. Furthermore, the relationship between $ln(sinh(\alpha\sigma_p)) - 1/T$ derived from the experimental peak stresses is plotted in Figure 8b. The average of the slopes at different strain rates S can be obtained, and the activation energy Q can be determined directly by Equation (9).
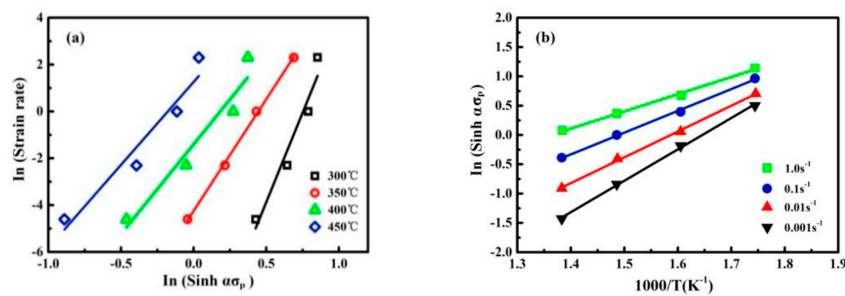
Figure 8. Relationship between (**a**) *ln E* and *ln(sinh(ασ_p))* and (**b**) *ln(sinh(ασ_p))* and 1000/T.

Figure 9 shows the relationship between V content and activation energy Q during hot deformation. It can be seen that the activation energy of the samples initially increases and then decreases with the increase of V content. The activation energy reaches its peak value (166 kJ/mol) when the V content is 0.05 wt.% (alloy C), which is about 10.0% higher than the base alloy. Afterward, the activation energy decreases, and when the V content is 0.1 wt.% (alloy D), the activation energy reduces to 155 kJ/mol, which is almost equivalent to that of the base alloy. Therefore, adding V of an appropriate amount to alloy 5083 can significantly increase the flow stress and peak stress during hot deformation. The experimental data are consistent with the literature (about 160 kJ/mol for AA 5083 with higher Fe and Si contents) [26], and the changes of activation energy show a similar tendency to the results obtained in another aluminum alloy [25], where an addition 0.05 wt.% of V in alloy 7150 led to an 18% increase of the activation energy Q as compared with the base alloy. This is a result of the solute drag effect of V on the dislocation slip and the restrained dynamic recovery, which causes the increase of deformation resistance. Meanwhile, the addition of 0.05 wt.% V results in a maximum Q value among the 7150 alloys studied with 0–0.15 wt.% V contents.
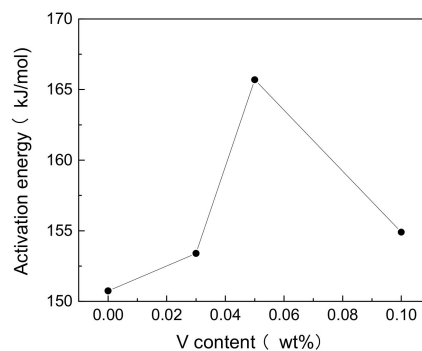
Figure 9. Relationship curve between thermal deformation activation energy Q and V content.

Processing maps are normally generated to determine the proper process domains for aluminum alloys. Figure 10 illustrates processing maps for alloy C in a temperature range of 300 to 450 °C and a strain rate range of 0.01 to 10 s^{-1} (log $\dot{\varepsilon}$ = −2 to 1) at a true strain of 0.2, 0.4 and 0.6 The contour lines in the maps represent the value of power dissipation, and the shaded areas in the maps indicate the unstable domains ($\xi < 0$) during thermal processing.

It is observed that the main unstable domains during deformation are situated in two domains, one is at high temperature and high strain rate (region I: temperature 390–440 °C and strain rate 1–10 s^{-1}), and the other one is at low temperature and middle strain rate (region II: temperature 300–330 °C and strain rate 0.03–0.3 s^{-1}). With the increase of true strain to 0.4, the unstable region I does not change obviously, while region II begins to expand and moves to the lower temperature and lower strain rate area gradually. When the true strain further increases to 0.6, region II tends to the higher strain rate area, and region I extends to the lower temperature area, which results in a unstable domain at a temperature range from 350 to 450 °C with strain rates of 1 to 10 s^{-1} (log$\dot{\varepsilon}$ = 0 to 1). At this time, the maximum value of power dissipation happens in the region within a temperature

range of 350–430 °C and strain rate of 0.01–0.030 s^{-1}. It can be expected that when deformed under these conditions, the alloy can show good hot working ability and cracking is not likely to occur. Such behavior is well related to the uniform microstructure of alloy C after deformation (Figure 4c).
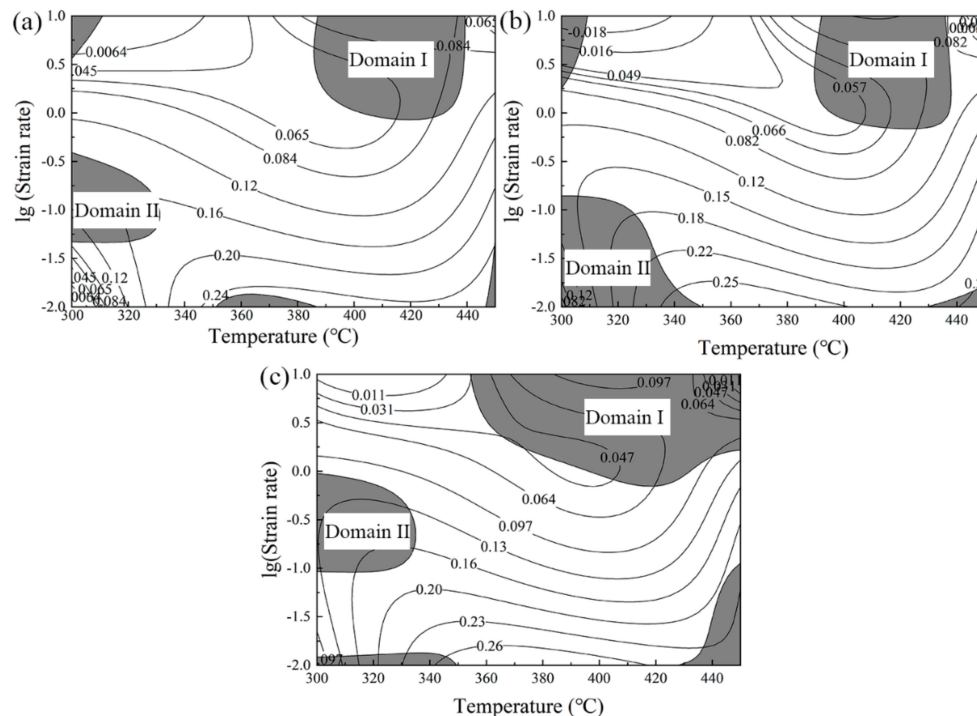
Figure 10. Processing maps of alloy C at various strains: (**a**) strain of 0.2, (**b**) strain of 0.4 and (**c**) strain of 0.6.

4. Conclusions

In this paper, the hot deformation behavior of aluminum alloy 5083 with different V contents was investigated. The main results can be summarized as follows:

(1) The addition of 0.05 wt.% V to alloy 5083 can increase the flow stress due to the existence of fine Al$_3$V particles formed during homogenization, which show a pinning effect on the dislocations and sub-grains during hot deformation processes.

(2) The activation energy of alloy 5083 changes with increasing V contents up to 0.05 wt.%. In the alloy with 0.05 wt.% V, the activation energy reaches the maximum value of 166 kJ/mol, which is 10.0% higher than that of V-free alloy 5083.

(3) For a higher true strain, the appropriate process domain for alloy C is in the temperature ranges of 350–430 °C and strain rates of 0.01–0.030 s^{-1}.

References

1. Yi, G.S.; Sun, B.H.; Poplawsky, J.D.; Zhu, Y.K.; Free, M.L. Investigation of pre-existing particles in Al 5083 alloys. *J. Alloys Compd.* **2018**, *740*, 461–469. [CrossRef]
2. Grajca, A.; Morawiec, M.; Zalecki, W. Austenite decomposition and precipitation behavior of plastically deformed low-Si microalloyed steel. *Metals* **2018**, *8*, 1028. [CrossRef]
3. Smith, D.; Joris, O.P.J.; Sankaran, A.; Weekes, H.E.; Bull, D.J.; Prior, T.J.; Dye, D.; Errandonea, D.; Proctor, J.E. On the high-pressure phases stability and elastic properties of β-titanium alloys. *J. Phys. Condens. Mater.* **2017**, *29*, 155401. [CrossRef] [PubMed]
4. Ling, O.; Zheng, Z.Q.; Nie, Y.F.; Jian, H.G. Hot deformation behavior of 2060 alloy. *J. Alloys Compd.* **2015**, *648*, 681–689.
5. Yan, L.M.; Shen, J.; Li, J.P.; Li, Z.B.; Tang, Z.L. Dynamic recrystallization of 7055 aluminum alloy during hot deformation. *Mater. Sci. Eng. A* **2010**, *650*, 295–301. [CrossRef]
6. Pan, S.P.; Chen, Y.Q.; Song, W.W. Effects of Initial Microstructure Characteristics on Hot De-formation Behaviors of 2E12 Aluminum Alloy. *J. Mater. Eng.* **2016**, *44*, 22–32. [CrossRef]
7. Koushki, A.R.; Goodarzi, M.; Paidar, M. Influence of shielding gas on the mechanical and metallurgical properties of DP-GMA-welded 5083-H321 aluminum alloy. *Int. J. Miner. Metall. Mater.* **2016**, *23*, 1416–1426. [CrossRef]
8. Shamsipur, A.; Anvari, A.; Keyvani, A. Improvement of microstructure and corrosion properties of friction stir welded AA5754 by adding Zn interlayer. *Int. J. Miner. Metall. Mater.* **2018**, *25*, 967–973. [CrossRef]
9. Fang, H.C.; Chao, H.; Chen, K.H. Effect of Zr, Er and Cr additions on microstructures and properties of Al–Zn–Mg–Cu alloys. *Mater. Sci. Eng. A* **2014**, *610*, 10–16. [CrossRef]
10. Wen, S.P.; Wang, W.; Zhao, W.H. Precipitation hardening and recrystallization behavior of AlMgErZr alloys. *J. Alloy. Compd.* **2016**, *687*, 143–151. [CrossRef]
11. Liu, R.; Hui, H.; Jun, M. Mechanical Properties at Low Temperature and Microstructure of Al-6Mg-0.8Zn-0.5Mn-0.2Zr-0.2Er Alloy. *Rare Met. Mater. Eng.* **2018**, *47*, 162–168.
12. Huang, P.P.; Somers, A.; Howlett, C. Film formation in trihexyl (tetradecyl) phosphonium diphenylphosphate ionic liquid on AA5083 aluminium alloy. *Surf. Coat. Technol.* **2016**, *303*, 385–395. [CrossRef]
13. Benallal, A.; Berstad, T.; Børvik, T. An experimental and numerical investigation of the behaviour of AA5083 aluminium alloy in presence of the Portevin–Le Chatelier effect. *Int. J. Plast.* **2008**, *24*, 1916–1945. [CrossRef]
14. Wen, S.P.; Gao, K.Y.; Huang, H. Role of Yb and Si on the precipitation hardening and recrystallization of dilute Al–Zr alloys. *J. Alloy. Compd.* **2014**, *599*, 65–70. [CrossRef]
15. Fan, C.H.; Chen, X.H.; Zhou, X.P. Microstructure evolution and strengthening mechanisms of spray-formed 5A12 Al alloy processed by high reduction rolling. *Trans. Nonferrous Met. Soc. China* **2017**, *27*, 2363–2370. [CrossRef]
16. Allen, C.M.; O'Reilly, K.A.Q.; Evans, P.V. The effect of vanadium and grain refiner additions on the nucleation of secondary phases in 1xxx Al alloys. *Acta Mater.* **1999**, *47*, 4387–4403. [CrossRef]
17. Kazakova, E.F.; Rusnyak, Y.I. A study of rapidly hardened aluminum alloys with iron and vanadium. *Met. Sci. Heat Treat.* **2009**, *51*, 436–439. [CrossRef]
18. Camero, S.; Puchi, E.S.; Gonzalez, G. Effect of 0.1% vanadium addition on precipitation behavior and mechanical properties of Al-6063 commercial alloy. *J. Mater. Sci.* **2006**, *41*, 7361–7373. [CrossRef]
19. Esquivel, J.; Gupta, R.K. Influence of the V content on microstructure and hardness of high-energy ball milled nanocrystalline Al-V alloys. *J. Alloy. Compd.* **2018**, *760*, 63–70. [CrossRef]
20. Shi, C.; Chen, X.G. Effect of vanadium on hot deformation and microstructural evolution of 7150 aluminum alloy. *Mater. Sci. Eng. A* **2014**, *613*, 91–102. [CrossRef]
21. Shi, C.; Chen, X.G. Evolution of activation energies for hot deformation of 7150 aluminum alloys with various Zr and V additions. *Mater. Sci. Eng. A* **2016**, *650*, 197–209. [CrossRef]
22. Brooks, S.P.; Gelman, A. General Methods for Monitoring Convergence of Iterative Simulations. *J. Comput. Graph. Stat.* **1998**, *7*, 434–455.
23. Yan, Y.; Qi, Y.; Chen, L.J. Strain rate dependent high temperature compressive deformation characteristics of ultrafine-grained pure aluminum produced by ECAP. *Trans. Nonferrous Met. Soc. China* **2016**, *26*, 966–973. [CrossRef]

24. Ramesh, K.T. Effects of high rates of loading on the deformation behavior and failure mechanisms of hexagonal close-packed metals and alloys. *Metall. Mater. Trans. A* **2002**, *33*, 927–935. [CrossRef]

25. Sherby, O.D.; Ruano, O.A. Rate-controlling processes in creep of subgrain containing aluminum materials. *Mater. Sci. Eng. A* **2005**, *410–411*, 8–11. [CrossRef]

26. Wu, W.X.; Sun, D.Q.; Cao, C.Y.; Wang, Z.F.; Zhang, H. Flow stress behavior of 5083 aluminium alloy under hot compression deformation. *Trans. Nonferrous Met. Soc. China* **2007**, *17*, 1667–1671.